Environmental Science: Atmospheres

ROYAL SOCIETY OF CHEMISTRY

PAPER

View Article Online
View Journal | View Issue

Cite this: *Environ. Sci.: Atmos.*, 2026, **6**, 551

Vertical profiles of NO_3 reactivity within the surface layer of a boreal forest

Patrick Dewald, [a] Simone T. Andersen, [a] Gunther N. T. E. Türk,[a] Laura Wüst,[a] Carolina Nelson, [a] Jan Schuladen,[a] Mikael Ehn,[b] Tuukka Petäjä, [b] Ilona Ylivinkka, [bc] Lauri R. Ahonen,[bc] Horst Fischer,[a] Jos Lelieveld[a] and John N. Crowley *[a]

The reaction of the nitrate radical (NO_3) with biogenic volatile organic compounds (BVOC) in the atmosphere is a significant source of secondary organic aerosols and can affect the reactive nitrogen budget. Field studies dedicated to NO_3-BVOC interaction on elevated platforms have highlighted vertical variability in both NO_3 and BVOC mixing ratios. While vertical profiles of NO_3 in the upper parts of the troposphere have been studied extensively, height-resolved measurements within the surface layer of BVOC-dominated areas, such as forests, are scarce. During the "Biosphere-Atmosphere Interactions and the Reactive Nitrogen Budget: Vertical Profiles of Key Species" (BAIRN-VIP) campaign, we measured vertical profiles of (B)VOC-induced NO_3 reactivity (k^{VOC}) along with the NO_3 precursors nitrogen dioxide (NO_2) and ozone (O_3) at five heights below the canopy (1–16 m) as well as at one height above it (28 m) in order to assess the vertical gradients of both NO_3 and BVOCs in the boreal forest of Hyytiälä, Finland. We find that the stability of the nocturnal boundary layer and decoupling of the sub-canopy flow are the main drivers of the vertical gradients in k^{VOC}. Steady-state calculations indicate that NO_3 concentrations on the order of pptv are found exclusively above the canopy during strongly decoupled nights, with BVOCs as the only NO_3 sink at heights above 4 m. During the day, BVOCs contribute, on average, 40–60% to the loss of NO_3 along the profile. Our results indicate that single-height field measurements of NO_3 are insufficient to explain nighttime oxidation chemistry under decoupled conditions.

Received 19th November 2025
Accepted 10th February 2026

DOI: 10.1039/d5ea00153f

rsc.li/esatmospheres

Environmental significance

The nocturnal oxidation of biogenic volatile organic compounds (BVOCs) by the nitrate radical (NO_3) has an impact on the reactive nitrogen budget. Despite the pronounced vertical gradients that these trace gases can exhibit at night, particularly within forested environments, height-resolved observations are scarce. Here, we present measurements of BVOC-induced NO_3 reactivity at several heights both above and below the canopy of a boreal forest. These observations provide new insights into the fate and vertical distribution of the NO_3 radical in this environment and further underscore the limitations and potential biases associated with more common single-height measurements.

1 Introduction

With an estimated area of *ca.* 15 million km^2, boreal forests cover a large fraction of the Earth's surface and contribute significantly to the ~1000 Tg $year^{-1}$ of biogenic volatile organic compounds (BVOCs), such as isoprene (2-methylbuta-1,3-diene, C_5H_8) and monoterpenes ($C_{10}H_{16}$) that are released into the atmosphere by vegetation.[1,2] The oxidation of BVOCs in the presence of nitric oxide (NO) and nitrogen dioxide (NO_2) is a well-known source of surface ozone (O_3)[3] and has a crucial impact on air quality and climate.[4,5] The major initiators of BVOC-oxidation in the troposphere are O_3, the hydroxyl radical (OH) and the nitrate radical (NO_3).[6,7] NO_3, the focus of this study, is produced from the sequential oxidation of NO and NO_2 by O_3 (R1, R2).[8] The nitrate radical is in thermal equilibrium with NO_2 and dinitrogen pentoxide (N_2O_5, R3a and R3b) and is present mainly at night, when it is not exposed to sunlight or high levels of NO.[9] The reaction with NO (R4) and photolysis (R5a and R5b) are important sinks of NO_3,[10] both of which reform NO_x (=NO + NO_2).

$$NO + O_3 \rightarrow NO_2 + O_2 \quad (R1)$$

$$NO_2 + O_3 \rightarrow NO_3 + O_2 \quad (R2)$$

[a]*Atmospheric Chemistry Department, Max Planck Institute for Chemistry, Mainz 55128, Germany. E-mail: john.crowley@mpic.de*

[b]*Institute for Atmospheric and Earth System Research/Physics, Faculty of Science, University of Helsinki, Helsinki, Finland*

[c]*Station for Measuring Ecosystem – Atmosphere Relations II (SMEAR II), University of Helsinki, Korkeakoski, 35500, Finland*

$$NO_2 + NO_3 + M \rightarrow N_2O_5 + M \quad \text{(R3a)}$$

$$N_2O_5 + M \rightarrow NO_3 + NO_2 + M \quad \text{(R3b)}$$

$$NO_3 + NO \rightarrow 2NO_2 \quad \text{(R4)}$$

$$NO_3 + h\nu \rightarrow NO + O_2 \quad \text{(R5a)}$$

$$NO_3 + h\nu \rightarrow NO_2 + O \quad \text{(R5b)}$$

The nitrate radical reacts with BVOCs (R6), leading to a variety of oxidation products including organic nitrates (*e.g.* $RONO_2$) or nitric acid (HNO_3),[11] which may be transferred to particulate matter or deposited on surfaces. Many studies report significant yields of both $RONO_2$ and secondary organic aerosol (SOA) from the NO_3-initiated oxidation of BVOCs.[12–18] In contrast to R4, R5a and R5b, the reaction between NO_3 and BVOCs (R6) opens the possibility of irreversible NO_x removal from the gas-phase, *e.g. via* organic nitrate deposition.[19,20] Reaction R6 is thus of particular interest to understand the impact of BVOCs and NO_3 on the NO_x budget.

$$NO_3 + BVOC \rightarrow \text{products } (e.g.\ RONO_2, HNO_3) \quad \text{(R6)}$$

For the reasons outlined above, nearly all ambient NO_3 measurements have been made at night. Close to the surface, the NO_3 mixing ratio and its variability can be strongly influenced by the stability of the nocturnal boundary layer (NBL).[9,21] When the ground cools due to the absence of insolation at nighttime, buoyancy-induced convective mixing is diminished so that the NBL may stratify,[22] resulting in strong vertical gradients in NO_3, which will remain obscure if sampling is conducted at a single height. Most vertical profiles of NO_3 reported so far were taken above the boundary layer or in non-forested settings[23–30] and height-resolved, nighttime measurements of BVOCs, NO_3 or the NO_3 reactivity within the first tens of meters of the troposphere (the surface layer), are scarce.[10,31–33] In forested regions, surface layer meteorology is distinctly complex and the trace gas composition above the canopy can differ drastically from that below,[33,34] especially when the NBL is stratified *e.g.* in the absence of turbulence induced by wind-shear.[35–37] This can result in a decoupling of the sub-canopy atmospheric flux from the above-canopy region of the NBL, also known as the "nighttime (flux) problem".[38]

To gain deeper insight into the height dependent NO_3-chemistry in a forest environment, we measured vertical profiles of VOC-induced NO_3 reactivity (k^{VOC}) along with mixing ratios of NO, NO_2, and O_3 in the boreal forest at Hyytiälä (Finland) over a period of ~1 month in September 2024. This set of measurements is used to derive height-dependent NO_3 mixing ratios *via* stationary-state calculations. As k^{VOC} is mainly driven by monoterpenes at this site and in other forests,[10,39,40] these measurements also provide insight into the vertical gradients of BVOCs. A comparison between k^{VOC} and non-speciated (total) monoterpene mixing ratios is presented in Andersen *et al.*[41] and summarized briefly in the SI (S1).

2 Methods

The BAIRN-VIP campaign took place at the Station for Measuring Forest Ecosystem–Atmosphere Relations II (SMEAR II) in the boreal forest at Hyytiälä, Finland, in September 2024. Hyytiälä forest is situated *ca.* 180 m above sea level and *ca.* 50 km northeast of Tampere (*ca.* 260 000 inhabitants), the nearest city in this area. The site is thus only minimally influenced by anthropogenic activity. Hyytiälä forest is composed of Scots pine (>60%), Norway spruce, aspen and birch with an average tree-top height of ~21 m.[42,43] The understory is dominated by lingonberry, bilberry, heather, wavy hair grass and mosses. We installed our measurement container along with an automated inlet system next to the permanent, 35 m tower in a small clearing (*ca.* 420 m^2).

2.1 Vertical profile measurements

Vertical profiles were obtained along a diagonal between the container and the tower (*ca.* 8 m distant) using a self-made, winch-driven, pulley system (HOIST8, Pallit) and an inlet-manifold equipped with rain protection and filters (PTFE, 2 μm pore size, Pall Corp.) to which the 30 m sampling lines (PFA, 1/4 inch outer diameter, Swagelok) of the instruments were connected.[41] A software-controlled routine sequentially moved the manifold between different sampling heights. Each cycle included 7 minute measurement periods at 1 m, 2 m, 4 m, 8 m, 16 m, and 28 m. At the end of the 42 minute cycle, the manifold returned directly to 1 m (in <1 min).

2.2 Meteorological data

The temperatures at 0.4 m, 1.5 m, 3.3 m, 5.8 m, 8.8 m, 16.8 m, 21.6 m and 27 m were measured at the SMEAR II mast, *ca.* 130 m away from the container area. These temperatures (and gradients therein) were consistent with those measured at the tower at heights of 2 m, 7 m, 12 m, 17 m, 22 m, 27 m and 32 m.[41]

At a height of 27 m on the mast, a sonic anemometer (Gill HS-50) provided horizontal wind speed (U), standard deviation in vertical wind speed (σ_w), the Obukhov length (L) and the friction velocity (u^*) which were used to calculate a decoupling parameter describing the exchange of above and below canopy air (see Section 3.2). This ancillary data is found in the SI (Fig. S2).

2.3 NO_3 reactivity

A flow-tube reactor coupled to a cavity ring-down spectrometer (CRDS) was used to determine the VOC-induced NO_3 reactivity k^{VOC}.[44] The instrument features a thermostated (30 °C), Teflon-coated (FEPD-121, Chemours) glass reactor to synthesize NO_3 *in situ via* the oxidation of NO with O_3 (R1, R2). The NO flow is 3–5 standard (STP) cm^3 per minute (sccm) from a bottle containing 1 parts per million by volume (ppmv) NO in N_2. O_3 is generated in a flow of 400 sccm synthetic air, which is passed through a cuvette illuminated with a low-pressure Hg lamp (active wavelength of 185 nm, Jelight, 78-2046-2). The flow is heated to 140 °C to dissociate N_2O_5 into NO_3 and NO_2 (R3b) and then

mixed with either synthetic air (zeroing mode) or ambient air. Synthetic air was provided by a compressor coupled to a zero-air generator (CAP180, Fuhr GmbH).

This mixture, typically containing 30–50 parts per trillion by volume (pptv) of NO_3, is directed through a Teflon-coated flowtube thermostated to 20 °C, where the air resides for 11 s. The effective reaction time was derived by calibrations in which a known amount of NO is added to zero air every 2 h. Finally, the air is sampled through the CRDS operated at 662 nm used to quantify the NO_3 exiting the flowtube. Titration of the NO_3 with NO (R4) allows determination of the "cavity baseline". The NO_3 reactivity is inferred from the comparison of NO_3 mixing ratios in synthetic air to those in ambient air, whereby ambient air and synthetic air are sequentially sampled for 20 min and 7 min, respectively.

As detailed in Liebmann *et al.*,[44] corrections are necessary *via* numerical simulations using IUPAC-recommended rate coefficients[45] and ambient measurements of NO, NO_2, and O_3. This correction allows us to account for the impact of R1 to R5b, as well as the wall loss of NO_3, and to separate the total NO_3 reactivity from that induced by VOCs (k^{VOC}). To exclude bias from ambient NO_3 and N_2O_5, the air is sampled through an uncoated 2 L glass flask for which the NO_3 and N_2O_5 transmission is zero. With the instrument operated at a flow rate of 3000 sccm, the combined flask and sampling line yielded an air residence time of approximately 45 s. To account for R1 during this period, ambient NO concentrations were corrected by factors ranging from 0.3 to 1 prior to use in the numerical simulations. A dynamic dilution system with synthetic air enables the measurement of NO_3 reactivities of up to *ca.* 2 s^{-1}. The lower limit of detection (LOD) during the campaign was 0.006 s^{-1} and was mainly driven by the (temperature-dependent) stability of both the NO_3 source and the cavity system. The latter induces a measurement uncertainty of 21%. The numerical simulation procedure introduces additional uncertainty that depends on the ratio of ambient NO_x to VOC concentrations. On average, the total systematic measurement uncertainty associated with k^{VOC} was 36% during this campaign.

2.4 NO, NO_2 and O_3

Measurements of both NO_2 and NO were provided by chemiluminescence detection of NO (ECO Physics CLD 790 CR) and photolytic conversion of NO_2 to NO.[46,47] Calibration of the sensitivity was performed every 2–3 days using an NO standard (5 ppmv in N_2, Air Liquide) and the conversion efficiency of the photolytic converter was determined 4 times during the campaign and remained stable. The effect of quenching of the NO_2* fluorescence by water (H_2O) was investigated in post-campaign laboratory experiments and accounted for using the measured relative humidity and temperature during the campaign. Background measurements were performed every 10 minutes by sampling through a pre-chamber while adding O_3. During this campaign, the LODs of NO and NO_2 were 4.5 and 17 pptv with associated uncertainties of 4 and 5%, respectively. O_3 mixing ratios (5% uncertainty, LOD of 2 ppbv) were measured with a commercial ozone monitor (2B Technologies, model 205) equipped with a UV absorption cell. The NO_x and O_3 instruments shared a common inlet line with a total sampling flow rate of ~10 000 sccm, corresponding to a residence time of approximately 1.7 s, during which minor chemical losses due to R1 may occur. Although larger corrections (up to ±20 pptv) occurred occasionally during daytime, nighttime corrections applied to NO and NO_2 to account for R1 were generally small, with 99% of NO corrections below 2 pptv and 97% of NO_2 corrections within ±3 pptv, well below the instrumental LODs.

2.5 Photolysis frequencies

A spectral radiometer (Metcon GmbH) installed on top of the tower at 38 m (*i.e.* above the tree-tops) measured the downwelling actinic flux. The latter was converted to NO_3 photolysis frequencies (J_{NO_3}) using evaluated cross-sections.[45] No corrections for upwelling radiation were made. In order to assess NO_3 photolysis below the tree-tops, the *J*-values were scaled by the ratio between two permanent photosynthetically active radiation (PAR) measurements below (0.6 m) and above (35 m) the canopy at the SMEAR II site. This approach takes advantage of the fact that the NO_3 radical is only photolysed by sunlight in the PAR region.[48] A comparison between the two PAR measurements and the above-canopy NO_3 photolysis rates derived from our actinic flux measurements on the tower is depicted in the SI (Fig. S3).

3 Results and discussion

An overview of the measurements during the BAIRN-VIP campaign at different sampling heights (*z*) is depicted in Fig. 1. The campaign took place in September 2024 during the summer–autumn transition and this period is marked by mild daytime temperatures of 285–297 K and nighttime temperatures of 280–285 K close to the ground. Based on the NO_3 photolysis frequencies, daylight was from 03:30 to 17:30 UTC (6:30–20:30 local time; white periods), with maximum values of $J_{NO_3} \sim 0.2$ s^{-1} under clear conditions above the canopy. Based on the comparison of PAR measurements above and below the canopy (see Section 2.5 and Fig. S3), J_{NO_3} is reduced on average by a factor of ~5 close to the ground within the forest.

The mixing ratios of NO and NO_2 were mostly below 0.2 ppbv and 1 ppbv, respectively, highlighting the remote location of the SMEAR II site. Daytime ozone levels of 20–30 ppbv were often reached, with occasional peaks at 60 ppbv (predominantly in the first half of the campaign). During nights with strong temperature inversion, when ground-level O_3 approached 0 ppbv, NO mixing ratios of several tens of pptv were detected. Vertical gradients in NO, NO_2 and O_3 were observed during most nights, and may be explained in terms of nocturnal NO soil emissions.[49–51]

The VOC-induced NO_3 reactivity (k^{VOC}) showed a significant diel variation with a mean reactivity of 0.047 s^{-1} across all heights during the day and higher values of 0.07 s^{-1} during the night for $z < 16$ m. 0.07 s^{-1} corresponds, for example, to α-pinene mixing ratios of 308 pptv and 456 pptv, respectively,

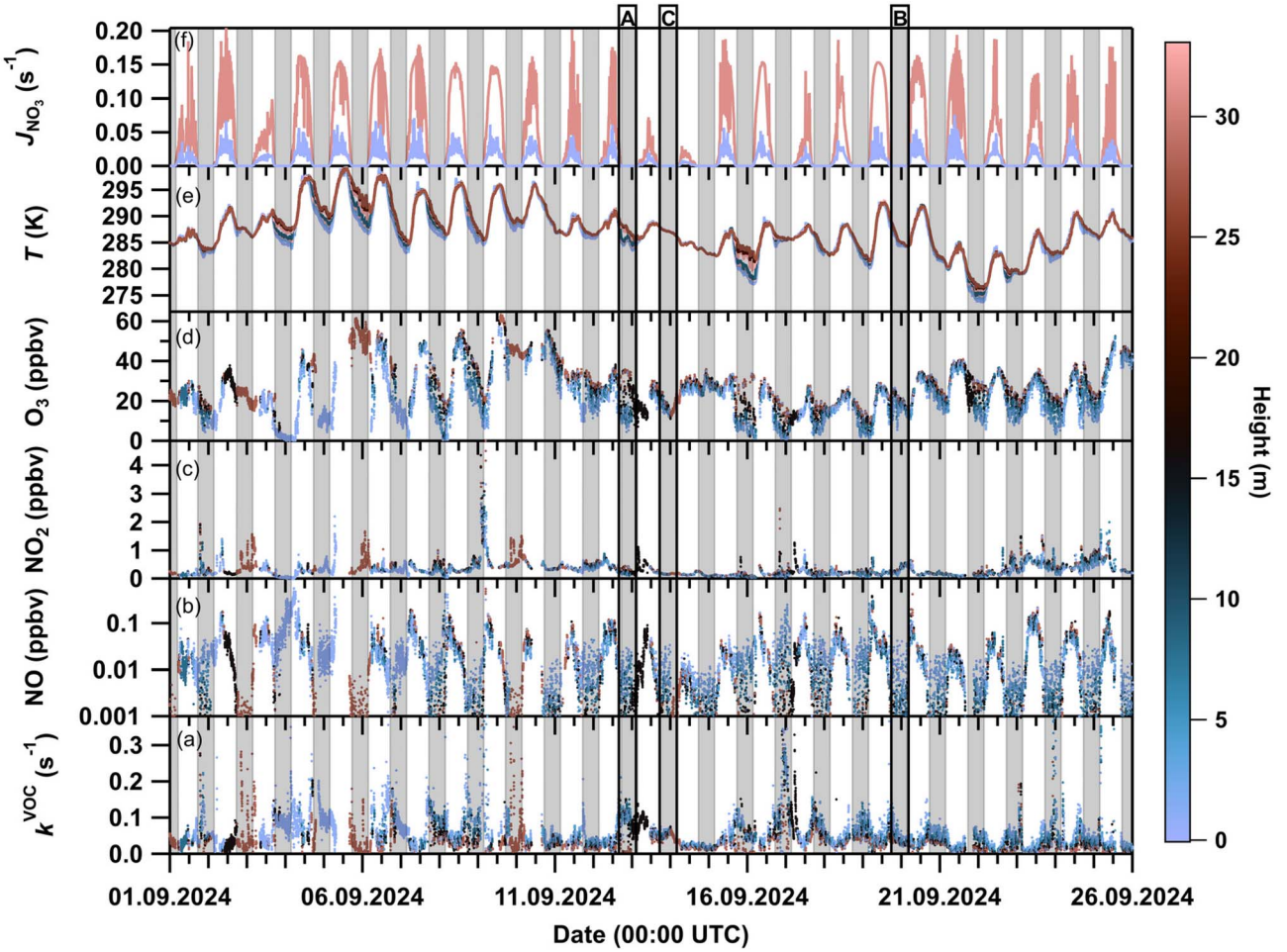

Fig. 1 Time series of VOC-induced NO_3 reactivity (k^{VOC}, a), nitric oxide (NO, b, log-scale), nitrogen dioxide (NO_2, c), ozone (O_3, d), temperature (T, e) and NO_3 photolysis frequencies (J_{NO_3}, f) during the BAIRN-VIP campaign. The data are colour-coded according to measurement height (colour scale on the right). The nighttime periods are shaded grey. The highlighted periods A, B, and C mark nights with extreme, moderate (typical condition for this campaign), and no temperature inversion, respectively.

a major constituent of monoterpenes at this site.[40] These observations are in line with the findings of Liebmann *et al.*,[10] who measured mean daytime and nighttime k^{VOC} values of 0.04 and 0.11 s^{-1}, respectively, at a height of 8 m in September 2016 at the same site. Below, we examine the vertical gradients of k^{VOC} and its drivers in more detail.

3.1 Vertical gradients in k^{VOC}

During BAIRN-VIP, we observed great night-to-night variability in the vertical gradients of k^{VOC} as well as significant changes within a single night. Zeroing as well as titration periods in the measurements of k^{VOC} resulted in data gaps in consecutive profile measurements. In order to account for these discontinuities, nocturnal k^{VOC} data were averaged over bins of *ca.* 1–2.5 h, ensuring that data from each height contributes similarly to the overall vertical profiles. The SI (S4) illustrates the evolution of the vertical k^{VOC} profile for each night. Note that even though we cannot rule out potential sampling losses of BVOCs, they are reported to be small in PFA lines.[52] Because all heights were sampled through the same line, any residual losses are expected to affect all levels equally and therefore are not expected to influence the observed vertical gradients significantly.

To identify key drivers of the gradient in NO_3 reactivity (*i.e.* BVOCs and NO), we focus on case studies and compare three different nights (marked by boxes in Fig. 1) with a "large" temperature inversion (Sep 12–13, period A), a "moderate" temperature inversion (Sep 20–21, period B) and "weak/no" temperature inversion (Sep 13–14, period C). The median vertical profiles at different times during these three nights are depicted in Fig. 2 (left panels). In addition, the NO_3 reactivity relative to that at 28 m at each sampling height is defined as f (right panels):

$$f(z) = \frac{k^{VOC}(z)}{k^{VOC}(28\ \mathrm{m})} \quad (1)$$

Around 17:30 on the night of Sep 12–13 (Fig. 2a) there was a "large" temperature inversion ($\Delta T = T_{27m} - T_{0.4m} \approx 3$ K) that diminished to ~2 K as the night progressed. The first two profiles (purple and blue lines) were very similar, with k^{VOC} at

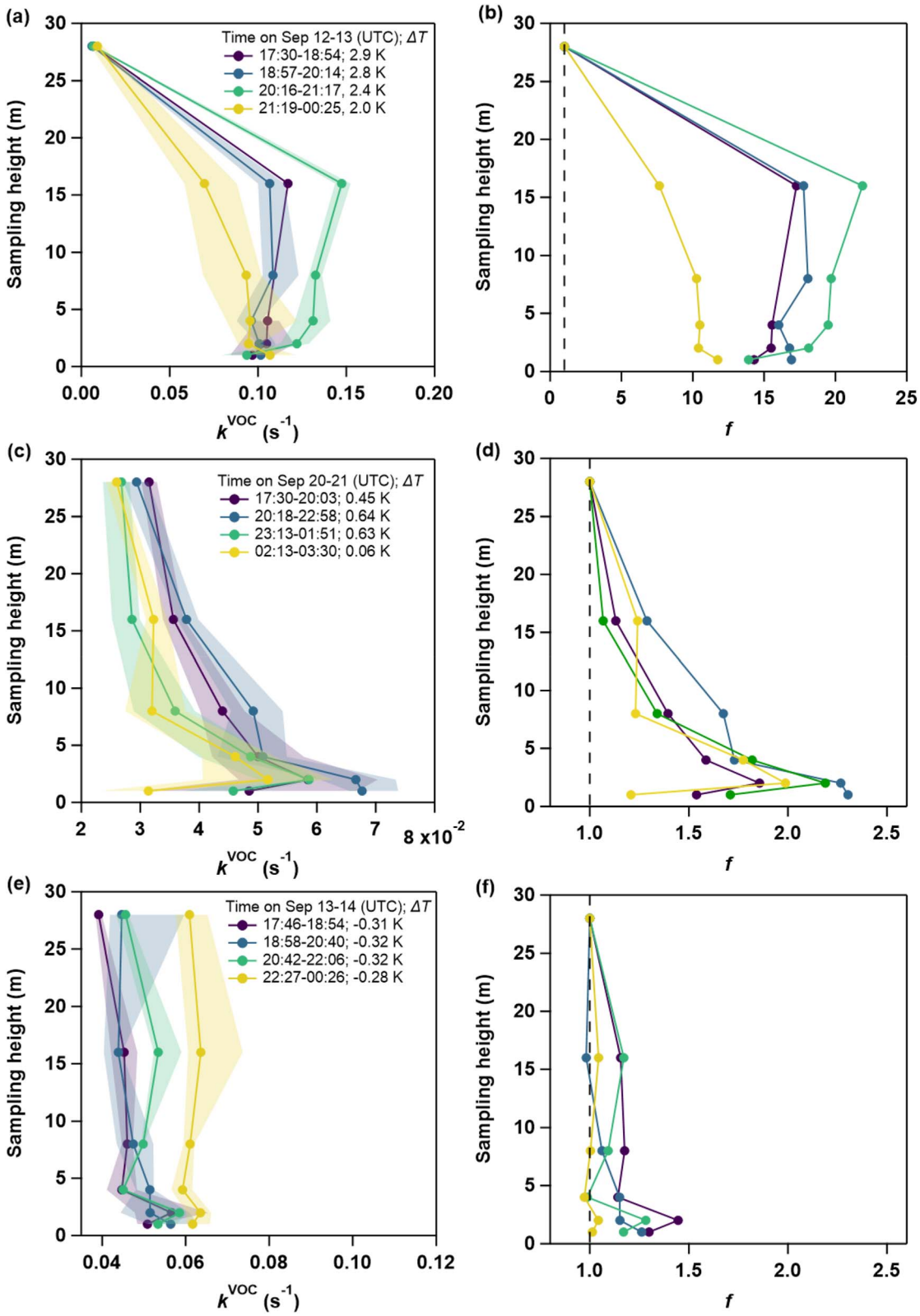

Fig. 2 Evolution of median vertical profiles of VOC-induced NO_3 reactivity from nights with (a) strong (period A), (c) moderate (period B) and (e) weak (period C) temperature inversion. The different time bins are coloured according to the legend that also includes the mean temperature inversions ($\Delta T = T_{27m} - T_{0.4\,m}$). The shaded areas denote the 25th and 75th percentiles. Panels (b), (d) and (f) show the fractional changes in NO_3 reactivity relative to 28 m (*f*, eqn (1)) for the corresponding night types. The dashed line marks zero gradient, *i.e.*, $f = 1$.

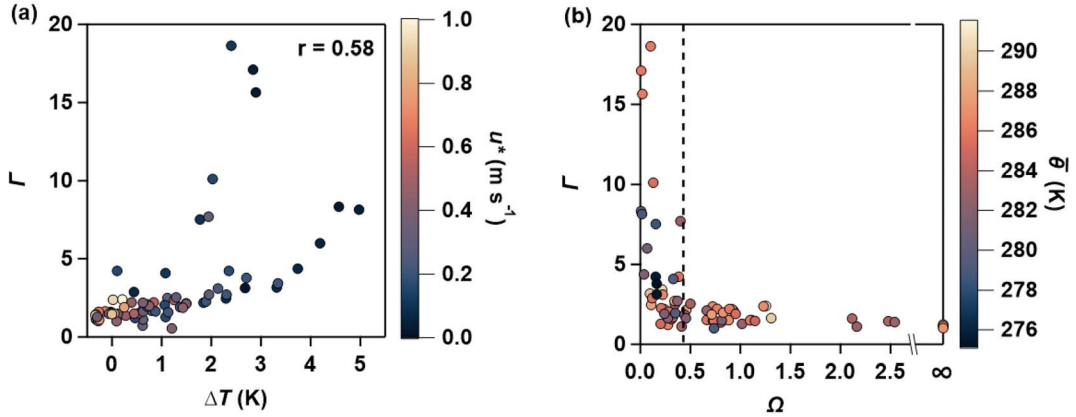

Fig. 3 (a) The mean vertical gradient in VOC-induced NO_3 reactivity (Γ, eqn (2)) plotted against the absolute temperature difference ($\Delta T = T_{27m} - T_{0.4m}$). The data is colour-coded by the mean friction velocity (u^*) at 27 m. Linear regression to the data results in a Pearson correlation coefficient (r) of 0.58. (b) Relationship between Γ and the decoupling parameter Ω (eqn (3)). The data is coloured by the mean, sub-canopy potential temperature (θ), according to the scale on the right.

ca. 0.1 s^{-1} between 1 m and 16 m, followed by a reduction to 0.007 s^{-1} at 28 m. As displayed in Fig. 2b, this corresponds to a fractional change f of ~16. During the fourth period (21:19–00:25 UTC, yellow) f was ~8–10. This decrease in f coincides with the weaker temperature inversion ($\Delta T \approx 2$ K). The consistently high values of f together with the persistently strong temperature gradient of 2–3 K, indicate decoupling of the sub-canopy from the above-canopy level (see Section 3.2), preventing air exchange between emission sources at the forest floor, understory and overstory as previously observed in forested environments.[36,38,53,54]

Fig. 2c shows a night (period B in Fig. 1) in which there was a "moderate" temperature inversion ($\Delta T \sim 0.5$ K) that persisted until 02:00 UTC. The values of k^{VOC} were between 0.03 s^{-1} and 0.07 s^{-1} and thus significantly lower compared to period A with a strong temperature inversion, possibly caused by a deeper boundary layer and thus lower monoterpene mixing ratios than in period A. Most of the profiles feature a local maximum k^{VOC} at a height of 2 m, which was observed on various other nights during the campaign (*e.g.* Sep 1–2, 14–15, 18–19, 23–24, 25–26, see SI S4). This feature can likely be attributed to two interacting processes: since the inlet system was set up in a clearing with a gravel surface, measurements made at 1 m may be influenced by different losses to and emissions from this surface compared to the understory of the surrounding forest at 2 m. In addition, Alekseychik *et al.*[53] reported the frequent presence of a drainage flow limited to the first few meters above ground level at this site. Its impact may be strongest closest to the surface, where coupling to the ground, deposition and near-surface advection are maximal, leading to greater decrease of k^{VOC} at 1 m than at 2 m. As presented in Fig. 2d, f varied between 1.5 and 2.2 until 01:51 UTC. Between 02:13 and 03:30 UTC, when the temperature gradient diminished, f decreased to 1.2 with the exception of the peak at 2 m.

The rainy night of Sep 13–14 (period C in Fig. 1) followed a rainy day, as reflected in less intense solar radiation (Fig. 1f), and no temperature inversion was apparent throughout the whole night. The vertical profiles of k^{VOC} are relatively flat on this night (Fig. 2e) with values between 0.04 and 0.06 s^{-1}, which are comparable to those observed in period B. The fractional change f (Fig. 2f) never exceeded 1.5 in period C, and between 22:27 and 00:26 UTC, f was close to 1.

3.2 Impact of atmospheric stability

The three case studies depicted in Fig. 2 show that the vertical profiles of atmospheric trace gases in the lowermost atmosphere are closely linked to temperature inversions. We have therefore examined the correlation between the temperature inversion and the vertical gradients in k^{VOC}. To do this, we define the mean of f (*i.e.* $\bar{f}$) for all sampling heights $z < 28$ m as the relative vertical gradient strength Γ of an averaged vertical profile:

$$\Gamma = \bar{f}(z),\ z < 28\ \text{m} \quad (2)$$

With this approach we account for the fact that the maximum value of f is not always at the same height and that while some profiles show a fairly continuous decrease in k^{VOC} with increasing height (*e.g.* period B, Fig. 2d), others do not (*e.g.* period A, Fig. 2b). To avoid distortion in the statistics, we omit nights lacking complete vertical profiles from the analysis. Fig. 3a plots Γ against the absolute temperature difference between 27 m and 0.4 m (ΔT). Extremely strong gradients with $\Gamma > 5$ occurred on the nights of Sep 12–13 (period A) and Sep (15–16), which are both characterized by strong temperature inversions ($\Delta T > 2$ K and >5 K, respectively). During nights with no or only a moderate temperature inversion ($\Delta T < 2$ K), Γ increases with ΔT, albeit with considerable scatter. A Pearson correlation analysis yields a correlation coefficient r of 0.58, which suggests that a significant fraction of the data scales linearly. The two nights with both high Γ and strong temperature inversion clearly do not follow this linear trend, implying that ΔT, serving as a measure for the local static stability of the nocturnal boundary layer, is not sufficient to evaluate the

overall stability. As mentioned above, from challenges encountered in the data evaluation of eddy flux measurements, it is well known that sub-canopy decoupling predominantly occurs during nights with stable stratification and low wind speeds.[35] This phenomenon has been observed at the SMEAR II site in previous studies.[53,55–57]

A common indicator for dynamic stability and decoupling used in the evaluation of flux measurements is a site-specific threshold value of the friction velocity (u^*),[58,59] which is, however, not necessarily applicable to all forested environments.[60,61] Colour-coding the data in Fig. 3a by u^* reveals that the two nights with high Γ (Sep 12–13 and Sep 15–16) are characterised by extremely low friction velocities above the canopy (blue points) and that higher friction velocities correspond to lower values of Γ and ΔT. A similar relationship between wind-induced mixing and vertical gradients of other species, such as O_3, has been reported in other forested environments.[62,63] However, using a friction velocity measured above the tree tops to evaluate the atmospheric stability of the sub-canopy may be problematic.[64]

Recently, Peltola *et al.*[55] introduced a universal meteorological decoupling parameter Ω, which takes forces opposing vertical mixing, such as buoyancy and canopy drag, into account. As explained in Peltola *et al.*[55] and Peltola *et al.*,[43] a temperature profile throughout the surface layer of the forest and the data set provided by an anemometer above the canopy (see Section 2.2) is sufficient to calculate an absolute critical vertical wind speed ($|w_{e,crit}(z)|$) that is necessary to move an air parcel from a measurement height z above the canopy to the ground. The stability parameter Ω is defined as the ratio between this critical wind speed and the standard deviation in vertical wind speed ($\sigma_w(z)$) as provided by the anemometer:

$$\Omega = \frac{\sigma_w(z)}{|w_{e,crit}(z)|} \quad (3)$$

In the SI (S2), we summarize the approach to derive $|w_{e,crit}(z)|$ by Peltola *et al.*,[43] who calculated this parameter using data at several measurement sites, including SMEAR II. They found that the sub-canopy starts to be weakly decoupled when Ω < 0.59. Assuming a Gaussian distribution of vertical wind speed fluctuations, the sub-canopy is clearly decoupled if Ω < 0.43.[55] Plotting Γ against Ω (Fig. 3b) confirms that, on the two exceptional nights with the highest gradients in k^{VOC} (Sep 12–13 and Sep 15–16), the in-canopy flow is strongly decoupled from the above-canopy flow as reflected in extremely low values of Ω (0.007–0.15). Γ steeply decreases as Ω increases from ~0 to 0.2. Strong gradients (Γ > 3) were never observed when Ω exceeded the threshold value for weak decoupling of 0.43 (dashed line in Fig. 3b). In the regime of Ω > 0.43, corresponding to conditions intermediate between weak decoupling and coupling, Γ maintained a mean value of approximately 1.5. On the night of Sep 13–14 (period C), with its characteristically weak gradients ($\Gamma \sim$ 1.2), Ω approaches infinity, *i.e.* unstable stratification due to ΔT < 0 as discussed in the previous section. It is important to note that the universal threshold values reported by Peltola *et al.*[43] may not be entirely suitable for our study, as we based our analysis on their mean leaf-area-index (LAI) of the Hyytiälä forest, but our measurements were taken in a clearing.

Fig. 3a and b strongly suggest that the meteorological stability of the lowermost atmosphere is an important driver of the gradient in k^{VOC}. However, even though the nights of Sep 12–13 and Sep 15–16 are qualitatively comparable, they show different Γ, despite having similar Ω. This emphasises the fact that other parameters may also affect Γ, including the emissions of trees, shrubs and soils. Since the monoterpene emission rates are temperature-dependent,[65] we colour-coded the data in Fig. 3b by the mean potential temperature in the sub-canopy (θ, z < 28 m). The lower value of Γ on Sep 15–16, compared to Sep 12–13, is seen to be accompanied by a lower temperature and therefore lower monoterpene emission rates.

In summary, Fig. 3 indicates that vertical gradients in k^{VOC} (or biogenic emissions) are mainly driven by surface layer stability, here quantified with Ω. However, the abundance of BVOCs is not only affected by their reaction with atmospheric oxidants (O_3, NO_3, OH) and the stability of the surface layer, but also by plant physiology.

3.3 Diel variability of vertical profiles

According to the results presented in Fig. 3b, nights can be classified into two regimes based on their nocturnal mean Ω: values exceeding 0.43 denote coupled conditions, whereas values below this threshold indicate decoupled conditions. Using this classification, we compare the vertical diel cycles of k^{VOC} in Fig. 4. Note that data from the day preceeding the night for which Ω was determined was used to generate the median

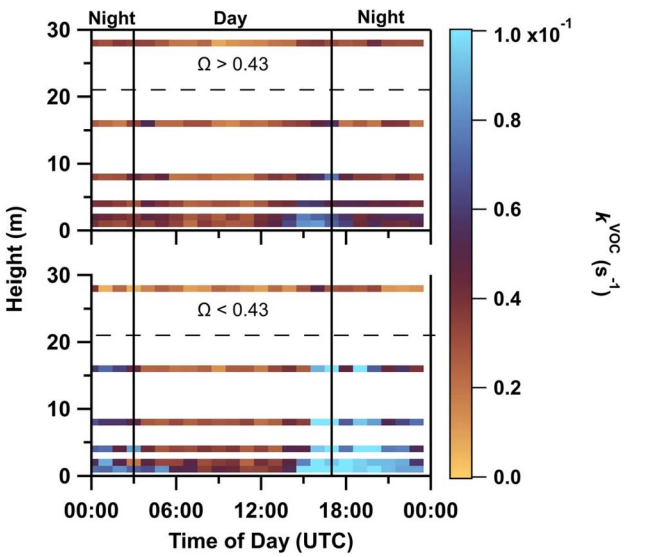

Fig. 4 Median diel cycles in VOC-induced NO_3 reactivity (k^{VOC}) plotted against sampling height and separated by the decoupling parameter Ω with Ω > 0.43 (upper panel) and Ω < 0.43 (lower panel). The highest NO_3 reactivities (light blue areas) are observed at the lowest heights under decoupling conditions (lower panel). The black vertical lines symbolise sunrise (03:00 UTC) and sunset (17:30 UTC) and the dashed black lines the tree top.

value k^{VOC} through the diel cycle. Furthermore, all nights shown in Fig. 1, including those without a complete vertical profile, were included in the analysis.

During nights with a coupled sub-canopy (upper panel in Fig. 4), only weak gradients were observed during the first half of the night between 17:30 and 22:00 UTC, with k^{VOC} reaching values ~0.05 s^{-1} close to the ground and decreasing to 0.03 s^{-1} above the canopy. Further into the night, the gradient diminished between 22:00 and 03:00 UTC and ground-level k^{VOC} decreased to ~0.04 s^{-1}. During the daytime, only weak vertical gradients (Γ) were observed until the late afternoon/early evening (15:00 UTC). This is consistent with an occasional daytime decoupling (as reflected in our calculated values of Ω) and a recent publication dealing with Ω at this site.[43] In order to avoid distortion of the statistics, daytime data impacted by local traffic and forestry activities as characterized by short-lived NO_x peaks were removed from the analysis.

Similarly, no strong vertical gradients (except during the dusk and dawn periods) occurred on the days preceding nights with a decoupled sub-canopy (Fig. 4, lower panel). In stark contrast to coupled conditions, very strong gradients were observed throughout the whole night. Sub-canopy reactivities were typically between 0.06 and 0.1 s^{-1}, whereas above-canopy values of k^{VOC} predominantly range from <0.006 s^{-1} to 0.02 s^{-1}.

3.4 The fate of the nitrate radical

We now further examine the impact of these two states, *i.e.* coupled and decoupled sub-canopy, on the abundance of the nitrate radical. As no height-dependent NO_3 measurements were available, we deduce NO_3 mixing ratios from a stationary-state approximation from the production (P) and loss (L) terms[33,66–69] whereby:

$$[NO_3]_{ss} \approx \frac{P}{L} \approx \frac{k_2[NO_2][O_3]}{k^{VOC} + k_4[NO] + J_{NO_3} + k_{het}} \quad (4)$$

and the terms in square parentheses are concentrations. k_2 is the rate coefficient for the reaction between O_3 and NO_2, k^{VOC} is the measured first-order loss coefficient, caused by reaction with VOCs, k_4 is the rate coefficient for the reaction between NO_3 and NO, J_{NO_3} is the NO_3 photolysis frequency, and k_{het} represents heterogeneous losses. As outlined in the SI (S5), k_{het}

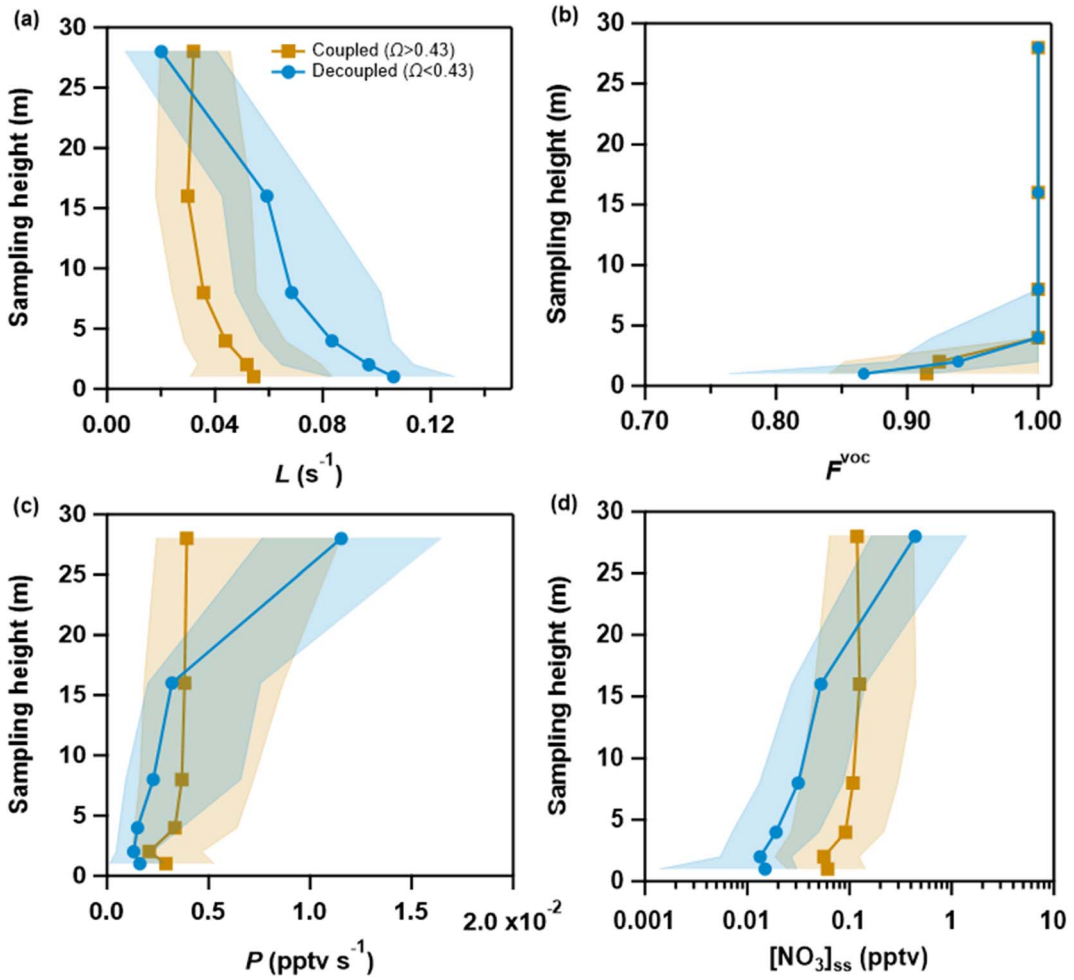

Fig. 5 Median vertical profiles at nighttime of (a) overall NO_3 loss rate coefficients (L), (b) fractional contribution of k^{VOC} to L (F^{VOC}), (c) NO_3 production rate (P) and (d) steady–steady mixing ratios of NO_3 ($[NO_3]_{ss}$) during nights with coupled (orange squares) and decoupled (blue circles) sub-canopy. The parameters were calculated with eqn (4) and (5). The 25th and 75th percentiles are shown by the shaded areas.

is negligible for this environment. To assess the fractional contribution F^{VOC} of VOC-induced NO_3 loss to the total loss term L, we use eqn (5):

$$F^{VOC} = \frac{k^{VOC}}{L} \quad (5)$$

As stated in the introduction, this NO_3 loss path is of particular interest, as it may efficiently remove NO_x from the gas phase.

3.4.1 Nighttime (17:30–03:30 UTC). The median vertical profiles of $[NO_3]_{ss}$, P, L and F^{VOC} at nighttime are displayed in Fig. 5. All campaign data were included, the orange squares are data obtained when the sub-canopy was coupled ($\Omega > 0.43$), the blue circles are data obtained when the sub-canopy was decoupled ($\Omega < 0.43$). During nights with coupled sub-canopy, only weak vertical gradients in L are observed (Fig. 5a, orange squares). Within the first 4−8 m above the ground-level, L decreased from *ca.* 0.05 s^{-1} to 0.03 s^{-1} and did not show any clear vertical variability above the tree-tops. This implies an average vertical gradient strength Γ of *ca.* 1.66 during coupled phases, which is in line with Fig. 3b. The vertical profiles of L during nights with a decoupled sub-canopy (Fig. 5a, blue circles) are in stark contrast to the observations during coupled conditions: L decreases continuously from 0.1 s^{-1} at 1 m to 0.02 s^{-1} at 28 m, with the greatest difference between 16 m and 28 m. Within the sub-canopy, L is higher during decoupled nights than during coupled ones. This opposing behaviour is reflected in the classification based on the decoupling parameter Ω and confirms that with intensifying vertical decoupling, BVOCs (and, at the lowest heights, also NO) accumulate in the sub-canopy. At the same time, reactions with VOCs are the only significant contributor to L during both types of night, with F^{VOC} approaching 1 at sampling heights $z > 2-4$ m (Fig. 5b). As a consequence, L drastically decreases above the canopy under decoupled conditions. Values of F^{VOC} that are less than 1 imply the presence of NO, which contributes less than 10% to L at sampling heights close to the ground (1−2 m) during coupled conditions (Fig. 5b). Under decoupled conditions, the NO contributions may increase to 25% at heights <4 m, which is related to low-level sources of NO such as soil and foliar surfaces.[51,70,71] NO mixing ratios above 4 m were limited by its reaction with O_3, and often at the detection limit of the measurement device.

During coupled nights, the NO_3 production rate P (Fig. 5c, orange squares) features only little vertical variability and increases from 0.003 to 0.004 pptv s^{-1} (*i.e.* by a factor of only 1.33). In contrast, under decoupled conditions, P increases from 0.0016 to 0.0032 pptv s^{-1} going from 1 m to 16 m within the canopy and sharply increases to 0.01 pptv s^{-1} at 28 m, which is well above the tree-tops. During decoupled nights P is smaller than under coupled conditions, which is related to lower O_3 mixing ratios resulting from higher deposition losses within a shallow boundary layer close to the ground.[72,73] Note that P in Fig. 5c is affected by the vertical gradients in both O_3 and NO_2, which are determined by boundary layer dynamics, heterogeneous processes and chemistry.[49,62,71] A detailed analysis of the vertical variability in NO, NO_2 and O_3 is beyond the scope of this work.

In summary, during both types of nights, the vertical profile of L is inverted compared to that of P. While the gradients are weak and mostly restricted to the ground and lower understory region (1–4 m) during coupled nights, much stronger and more continuous gradients with a distinct augmentation between the central overstory (16 m) and the above-canopy region (28 m) appear to be the signature feature of decoupled nights.

These differences also become evident in NO_3 mixing ratios (Fig. 5d) deduced from eqn (4). Due to the lower values of L and higher values of P in the sub-canopy during coupled conditions, $[NO_3]_{ss}$ (0.05–0.1 pptv) was significantly higher than in the decoupled sub-canopy ($[NO_3]_{ss}$ = 0.01–0.05 pptv). The median $[NO_3]_{ss}$ increases sharply to *ca.* 0.5 pptv above the canopy at 28 m under decoupled conditions. Generally, the high BVOC mixing ratios, as reflected in high values of k^{VOC} together with the absence of strong (anthropogenic) NO_2 sources, lead to low NO_3 mixing ratios at this site. On exceptional (strongly decoupled) nights with $\Omega < 0.01$, for example during the night of Sep 5–6, steady-state NO_3 mixing ratios of up to 8 pptv were calculated at 28 m. This is readily understood as, under decoupled conditions, BVOCs are constrained to lower heights (<21 m) whereas O_3 and NO_2 (and thus values of P) increase. This was confirmed by a direct NO_3 measurement (CRDS) of several tens of pptv of NO_3 on top of the neighbouring tower at 36 m, which will be reported elsewhere.

3.4.2 Daytime (03:30–17:30 UTC). Fig. 6a shows the campaign-averaged vertical profiles of $[NO_3]_{ss}$, P and L during the day. For heights above the canopy, J_{NO_3} was taken from actinic flux measurements at 38 m. For heights lower than the tree-tops, J_{NO_3} was derived from the ratio of PAR measurement close to the ground and above the canopy and scaling to J_{NO_3} at 38 m (see Section 2.5 and S3). As discussed by Bohn,[74] the vertical variability in photolysis frequencies is less of an issue if the vertical mixing time (τ_m) is shorter than the (photo)chemical lifetime (τ_c) of a species. The chemical lifetime of the nitrate radical is $1/L$, *i.e.* τ_c equals approximately 11 s at daytime. The mixing time can be approximated by z/u^*,[64] which using the daytime, campaign median value of u^* (at 27 m) of 0.46 m s^{-1}, results in a mixing time of approximately one minute. However, it should be kept in mind that the above-canopy measurement of the friction velocity does not necessarily represent the conditions below the canopy.

When taking the difference in J_{NO_3} above and below canopy into account, the total NO_3 loss term (the green line in Fig. 6a, top axis), shows only a weak vertical gradient during the day with L equal to 0.091 s^{-1} at 1 m and 0.086 s^{-1} at 28 m. Fig. 6b depicts the fractional contributions (F) of VOCs, NO and photolysis to L and shows that, while L exhibits no significant gradient, the different contributing loss processes do. Below the canopy ($z < 28$ m), the main loss pathway of NO_3 is reaction with VOCs (~60%), with photolysis and NO each contributing ~20%. Above the canopy, the contribution of NO remains at *ca.* 20%, whereas both photolysis and VOCs each account for 40%. This is due to both the increase in J_{NO_3} and the decrease (by 66%) in k^{VOC} above the canopy top. This gradient is not caused solely by reduced vertical mixing (the threshold value of $\Gamma \sim 1.5$, applies to both coupled nights and daytime, see Fig. 3b) but may result

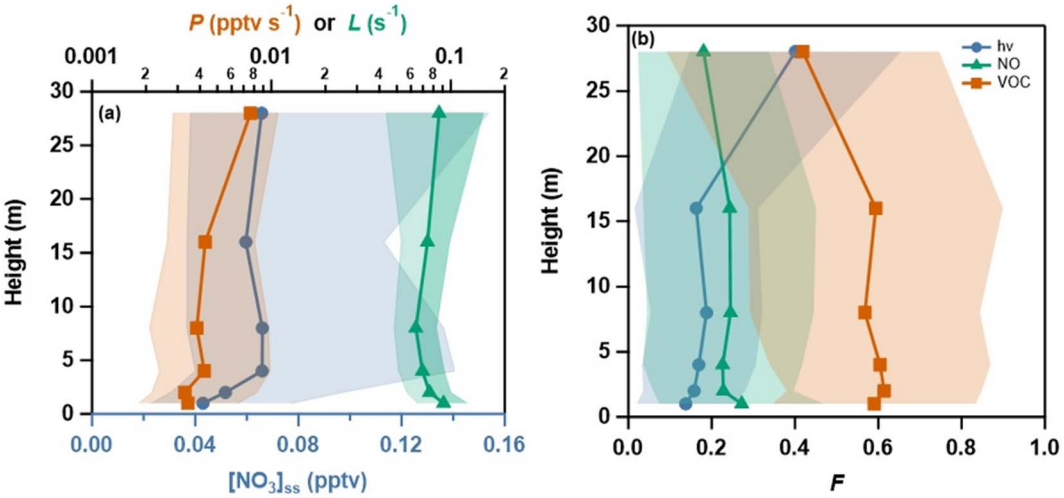

Fig. 6 (a) Campaign-average (median) vertical profiles of overall NO_3 loss rate coefficients (L, green triangles, denominator in eqn (4)), NO_3 production rate (P, orange squares) and steady–steady mixing ratios of NO_3 ($[NO_3]_{ss}$, grey-blue circles) during the day. (b) Median fractional contributions (F) by photolysis (blue circles), NO (green triangles) and VOCs (orange squares) to daytime L. In both panels, the 25th and 75th percentiles are shown by shaded areas.

from changes in the proximity to direct BVOC sources,[75,76] higher OH concentrations[77] or a lower surface area for deposition.

The production rate P (Fig. 6a, orange squares, top axis) is only 0.004 pptv s^{-1} below the canopy but doubles to 0.008 pptv s^{-1} above the canopy. Daytime values of P are similar to those during decoupled nights, which is related to different factors controlling the NO_2 mixing ratios. During decoupled nights, NO_2 in the sub-canopy is lost to surfaces,[39,49,78] whereas above the canopy during the day NO_2 is rapidly photolysed.[74]

Daytime, steady-state NO_3 mixing ratios (eqn (4)) are very low (Fig. 6a, grey-blue circles, bottom axis) and below the present-day limit of detection for *e.g.* CRDS instruments.[6] There is a slight increase within the first 4 m from 0.04 pptv to 0.065 pptv due to an increase in P and a decrease in L. While VOCs represent the primary sink of NO_3, such low NO_3 mixing ratios would contribute only marginally to the daytime oxidation of BVOCs, which is dominated by reactions with OH and O_3. Using IUPAC recommended rate coefficients[45] and typical midday levels of O_3 (*ca.* 31 ppbv) and OH (2.7×10^6 molecule cm^{-3} as inferred from UV-B radiation according to Hellén *et al.*[40]), only 2.7% of α-pinene oxidation is initiated by the NO_3 radical. However, the NO_3-initiated oxidation of monoterpenes can still significantly contribute to the formation of organic nitrates when the corresponding yields are taken into account.[18]

4 Summary and conclusions

Vertical profiles of VOC-induced NO_3 reactivity below and above the canopy were measured in September 2024 during the summer–autumn transition in the boreal forest of Hyytiälä, Finland. The surface layer stability, as represented by the decoupling parameter (Ω), was found to have a central impact on the vertical inter-canopy gradients (Γ) in k^{VOC}. In general, extremely strong gradients ($\Gamma > 3$) go hand in hand with exceptionally strong decoupling of the sub-canopy ($\Omega < 0.2$) from the rest of the nocturnal boundary layer. Even under coupled conditions ($\Omega > 0.43$), which typically prevail during most of the daytime or overcast nights, Γ generally attained values between 1.2 and 1.6.

Steady-state calculated mixing ratios of NO_3 exceed 0.5 pptv only above the canopy (28 m) during highly decoupled nights ($\Omega \approx 0$). VOCs are the major sink of NO_3 throughout the surface layer during the night, and on average contribute 40–60% to daytime NO_3 losses. Due to the low abundance of NO_x and low NO_3 production rates, the contribution of NO_3 to the daytime oxidation of VOCs remains minor, though.

This work highlights the importance of measuring vertical gradients of key trace gases and radicals in understanding the chemistry of both the nocturnal surface layer, where temperature inversions and vertical gradients are highly variable, but also the sub-canopy daytime boundary layer close to the ground in forested regions.

Author contributions

Patrick Dewald: data curation; formal analysis; investigation; methodology; visualization; writing – original draft; writing – review & editing. Simone T. Andersen: data curation; formal analysis; writing – review & editing. Gunther N. T. E. Türk: data curation; formal analysis; writing – review & editing. Laura Wüst: data curation; formal analysis; writing – review & editing. Carolina Nelson: data curation; formal analysis; writing – review & editing. Jan Schuladen: data curation; formal analysis; project administration. Mikael Ehn: project administration; validation; writing – review & editing. Tuukka Petäjä: data curation; project administration; validation; writing – review & editing. Ilona Ylivinkka: data curation; formal analysis; writing – review & editing. Lauri R. Ahonen: data curation; formal analysis; writing – review & editing. Horst Fischer: investigation; validation;

writing – review & editing. John N. Crowley: conceptualization; supervision; validation; writing – review & editing. Jos Lelieveld: resources; supervision; validation; writing – review & editing.

Conflicts of interest

The authors declare that they have no conflicts of interest.

Data availability

The meteorological data from the mast is accessible through the Fairdata services at https://doi.org/10.23729/fd-933fd9fd-d31b-3e26-a01b-acef7901b843.[79] Measurements of NO_3 reactivity, O_3, NO_x, and the sum of monoterpenes are available at Edmond (https://doi.org/10.17617/3.PBGFBI).[80]

Supplementary information (SI) is available. See DOI: https://doi.org/10.1039/d5ea00153f.

Acknowledgements

JNC acknowledges Chemours for the provision of a FEPD-121 sample used to coat the flowtube and the Deutsche Forschungsgemeinschaft for partial financial support (project "MONOTONS", project number: 522970430). STA thanks the Alexander von Humboldt foundation for funding her stay at the MPIC. This work was financially supported *via* the ATMO-ACCESS Trans National Access program under ATMO-TNA-3-0000000024 (NORACHO) and ATMO-TNA-7-0000000016 (BAIRN-VIP). The authors want to thank Uwe Parchatka (MPIC) and the SMEAR II team for their support throughout the campaign as well as ACTRIS for the monoterpene measurements with Vocus PTR-TOF. We also thank Üllar Rannik for the provision of valuable comments to this work. Scientific colour maps as provided by Crameri[81] are used in this study to prevent visual distortion of the data and exclusion of readers with colour-deficiencies. Open Access funding provided by the Max Planck Society.

References

1 G. Eerdekens, N. Yassaa, V. Sinha, P. P. Aalto, H. Aufmhoff, F. Arnold, V. Fiedler, M. Kulmala and J. Williams, VOC measurements within a boreal forest during spring 2005: on the occurrence of elevated monoterpene concentrations during night time intense particle concentration events, *Atmos. Chem. Phys.*, 2009, **9**, 8331–8350.

2 A. B. Guenther, X. Jiang, C. L. Heald, T. Sakulyanontvittaya, T. Duhl, L. K. Emmons and X. Wang, The Model of Emissions of Gases and Aerosols from Nature version 2.1 (MEGAN2.1): an extended and updated framework for modeling biogenic emissions, *Geosci. Model. Dev.*, 2012, **5**, 1471–1492.

3 P. J. Crutzen and J. Lelieveld, Human impacts on atmospheric chemistry, *Annu. Rev. Earth Planet. Sci.*, 2001, **29**, 17–45.

4 W. L. Chameides, F. Fehsenfeld, M. O. Rodgers, C. Cardelino, J. Martinez, D. Parrish, W. Lonneman, D. R. Lawson, R. A. Rasmussen, P. Zimmerman, J. Greenberg, P. Mlddleton and T. Wang, Ozone precursor relationships in the ambient atmosphere, *J. Geophys. Res. Atmos.*, 1992, **97**, 6037–6055.

5 B. N. Duncan, Y. Yoshida, J. R. Olson, S. Sillman, R. V. Martin, L. Lamsal, Y. Hu, K. E. Pickering, C. Retscher, D. J. Allen and J. H. Crawford, Application of OMI observations to a space-based indicator of NO_x and VOC controls on surface ozone formation, *Atmos. Environ.*, 2010, **44**, 2213–2223.

6 N. L. Ng, S. S. Brown, A. T. Archibald, E. Atlas, R. C. Cohen, J. N. Crowley, D. A. Day, N. M. Donahue, J. L. Fry, H. Fuchs, R. J. Griffin, M. I. Guzman, H. Herrmann, A. Hodzic, Y. Iinuma, J. L. Jimenez, A. Kiendler-Scharr, B. H. Lee, D. J. Luecken, J. Mao, R. McLaren, A. Mutzel, H. D. Osthoff, B. Ouyang, B. Picquet-Varrault, U. Platt, H. O. T. Pye, Y. Rudich, R. H. Schwantes, M. Shiraiwa, J. Stutz, J. A. Thornton, A. Tilgner, B. J. Williams and R. A. Zaveri, Nitrate radicals and biogenic volatile organic compounds: oxidation, mechanisms, and organic aerosol, *Atmos. Chem. Phys.*, 2017, **17**, 2103–2162.

7 P. O. Wennberg, K. H. Bates, J. D. Crounse, L. G. Dodson, R. C. McVay, L. A. Mertens, T. B. Nguyen, E. Praske, R. H. Schwantes, M. D. Smarte, J. M. St Clair, A. P. Teng, X. Zhang and J. H. Seinfeld, Gas-Phase Reactions of Isoprene and Its Major Oxidation Products, *Chem. Rev.*, 2018, **118**, 3337–3390.

8 R. P. Wayne, I. Barnes, P. Biggs, J. P. Burrows, C. E. Canosamas, J. Hjorth, G. Lebras, G. K. Moortgat, D. Perner, G. Poulet, G. Restelli and H. Sidebottom, The Nitrate Radical - Physics, Chemistry, and the Atmosphere, *Atmos. Env. A*, 1991, **25A**, 1–203.

9 S. S. Brown and J. Stutz, Nighttime radical observations and chemistry, *Chem. Soc. Rev.*, 2012, **41**, 6405–6447.

10 J. Liebmann, E. Karu, N. Sobanski, J. Schuladen, M. Ehn, S. Schallhart, L. Quéléver, H. Hellen, H. Hakola, T. Hoffmann, J. Williams, H. Fischer, J. Lelieveld and J. N. Crowley, Direct measurement of NO_3 radical reactivity in a boreal forest, *Atmos. Chem. Phys.*, 2018, **18**, 3799–3815.

11 B. J. Finlayson-Pitts and J. N. Pitts, in *Chemistry of the Upper and Lower Atmosphere*, Academic Press, San Diego, 2000, pp. 264–293, DOI: 10.1016/B978-012257060-5/50009-5.

12 J. L. Fry, A. Kiendler-Scharr, A. W. Rollins, T. Brauers, S. S. Brown, H. P. Dorn, W. P. Dube, H. Fuchs, A. Mensah, F. Rohrer, R. Tillmann, A. Wahner, P. J. Wooldridge and R. C. Cohen, SOA from limonene: role of NO_3 in its generation and degradation, *Atmos. Chem. Phys.*, 2011, **11**, 3879–3894.

13 K. H. Bates, G. J. P. Burke, J. D. Cope and T. B. Nguyen, Secondary organic aerosol and organic nitrogen yields from the nitrate radical (NO_3) oxidation of alpha-pinene from various RO_2 fates, *Atmos. Chem. Phys.*, 2022, **22**, 1467–1482.

14 C. M. Boyd, J. Sanchez, L. Xu, A. J. Eugene, T. Nah, W. Y. Tuet, M. I. Guzman and N. L. Ng, Secondary organic aerosol formation from the beta-pinene + NO_3 system:

effect of humidity and peroxy radical fate, *Atmos. Chem. Phys.*, 2015, **15**, 7497–7522.
15 A. W. Rollins, A. Kiendler-Scharr, J. L. Fry, T. Brauers, S. S. Brown, H. P. Dorn, W. P. Dubé, H. Fuchs, A. Mensah, T. F. Mentel, F. Rohrer, R. Tillmann, R. Wegener, P. J. Wooldridge and R. C. Cohen, Isoprene oxidation by nitrate radical: alkyl nitrate and secondary organic aerosol yields, *Atmos. Chem. Phys.*, 2009, **9**, 6685–6703.
16 D. A. Day, J. L. Fry, H. G. Kang, J. E. Krechmer, B. R. Ayres, N. I. Keehan, S. L. Thompson, W. W. Hu, P. Campuzano-Jost, J. C. Schroder, H. Stark, M. P. DeVault, P. J. Ziemann, K. J. Zarzana, R. J. Wild, W. P. Dube, S. S. Brown and J. L. Jimenez, Secondary Organic Aerosol Mass Yields from NO_3 Oxidation of alpha-Pinene and Delta-Carene: Effect of RO_2 Radical Fate, *J. Phys. Chem. A*, 2022, **126**, 7309–7330.
17 M. P. DeVault, A. C. Ziola and P. J. Ziemann, Products and Mechanisms of Secondary Organic Aerosol Formation from the NO_3 Radical-Initiated Oxidation of Cyclic and Acyclic Monoterpenes, *ACS Earth Space Chem.*, 2022, **6**, 2076–2092.
18 J. Liebmann, N. Sobanski, J. Schuladen, E. Karu, H. Hellen, H. Hakola, Q. Zha, M. Ehn, M. Riva, L. Heikkinen, J. Williams, H. Fischer, J. Lelieveld and J. N. Crowley, Alkyl nitrates in the boreal forest: formation via the NO_3-, OH- and O_3-induced oxidation of biogenic volatile organic compounds and ambient lifetimes, *Atmos. Chem. Phys.*, 2019, **19**, 10391–10403.
19 P. S. Romer Present, A. Zare and R. C. Cohen, The changing role of organic nitrates in the removal and transport of NO_x, *Atmos. Chem. Phys.*, 2020, **20**, 267–279.
20 E. C. Browne, K. E. Min, P. J. Wooldridge, E. Apel, D. R. Blake, W. H. Brune, C. A. Cantrell, M. J. Cubison, G. S. Diskin, J. L. Jimenez, A. J. Weinheimer, P. O. Wennberg, A. Wisthaler and R. C. Cohen, Observations of total $RONO_2$ over the boreal forest: NO_x sinks and HNO_3 sources, *Atmos. Chem. Phys.*, 2013, **13**, 4543–4562.
21 J. Zhang and S. T. Rao, The Role of Vertical Mixing in the Temporal Evolution of Ground-Level Ozone Concentrations, *J. Appl. Meteorol.*, 1999, **38**, 1674–1691.
22 R. Stull, *Practical Meteorology: an Algebra-Based Survey of Atmospheric Science*, University of British Columbia, Vancouver, 2017.
23 J. P. Smith, S. Solomon, R. W. Sanders, H. L. Miller, L. M. Perliski, J. G. Keys and A. L. Schmeltekopf, Atmospheric NO_3: 4. Vertical Profiles at Middle and Polar Latitudes at Sunrise, *J. Geophys. Res. Atmos.*, 1993, **98**, 8983–8989.
24 C. von Friedeburg, T. Wagner, A. Geyer, N. Kaiser, B. Vogel, H. Vogel and U. Platt, Derivation of tropospheric NO_3 profiles using off-axis differential optical absorption spectroscopy measurements during sunrise and comparison with simulations, *J. Geophys. Res. Atmos.*, 2002, **107**, 4168.
25 J. Stutz, B. Alicke, R. Ackermann, A. Geyer, A. White and E. Williams, Vertical profiles of NO_3, N_2O_5, O_3, and NO_X in the nocturnal boundary layer: 1. Observations during the Texas Air Quality Study 2000, *J. Geophys. Res. Atmos.*, 2004, **109**, D12306.
26 S. S. Brown, W. P. Dube, H. D. Osthoff, J. Stutz, T. B. Ryerson, A. G. Wollny, C. A. Brock, C. Warneke, J. A. De Gouw, E. Atlas, J. A. Neuman, J. S. Holloway, B. M. Lerner, E. J. Williams, W. C. Kuster, P. D. Goldan, W. M. Angevine, M. Trainer, F. C. Fehsenfeld and A. R. Ravishankara, Vertical profiles in NO_3 and N_2O_5 measured from an aircraft: Results from the NOAA P-3 and surface platforms during the New England Air Quality Study 2004, *J. Geophys. Res. Atmos.*, 2007, **112**, D22304.
27 Y. H. Yan, S. S. Wang, J. Zhu, Y. L. Guo, G. Q. Tang, B. X. Liu, X. X. An, Y. S. Wang and B. Zhou, Vertically increased NO_3 radical in the nocturnal boundary layer, *Sci. Total Environ.*, 2021, **763**, 142969.
28 H. Zhang, Y. Zhang, Z. Huang, W. J. F. Acton, Z. Wang, E. Nemitz, B. Langford, N. Mullinger, B. Davison, Z. Shi, D. Liu, W. Song, W. Yang, J. Zeng, Z. Wu, P. Fu, Q. Zhang and X. Wang, Vertical profiles of biogenic volatile organic compounds as observed online at a tower in Beijing, *J. Environ. Sci.*, 2020, **95**, 33–42.
29 Y. Liu, H. Wang, S. Jing, M. Zhou, S. Lou, K. Qu, W. Qiu, Q. Wang, S. Li, Y. Gao, Y. Liu, X. Li, Z.-R. Peng, J. Chen and K. Lu, Vertical Profiles of Volatile Organic Compounds in Suburban Shanghai, *Adv. Atmos. Sci.*, 2021, **38**, 1177–1187.
30 D. J. Fish, D. E. Shallcross and R. L. Jones, The vertical distribution of NO_3 in the atmospheric boundary layer, *Atmos. Environ.*, 1999, **33**, 687–691.
31 S. S. Brown, W. P. Dube, H. D. Osthoff, D. E. Wolfe, W. M. Angevine and A. R. Ravishankara, High resolution vertical distributions of NO_3 and N_2O_5 through the nocturnal boundary layer, *Atmos. Chem. Phys.*, 2007, **7**, 139–149.
32 R. Petersen, T. Holst, M. Mölder, N. Kljun and J. Rinne, Vertical distribution of sources and sinks of volatile organic compounds within a boreal forest canopy, *Atmos. Chem. Phys.*, 2023, **23**, 7839–7858.
33 P. Dewald, T. Seubert, S. T. Andersen, G. N. T. E. Türk, J. Schuladen, M. R. McGillen, C. Denjean, J. C. Etienne, O. Garrouste, M. Jamar, S. Harb, M. Cirtog, V. Michoud, M. Cazaunau, A. Bergé, C. Cantrell, S. Dusanter, B. Picquet-Varrault, A. Kukui, C. Xue, A. Mellouki, J. Lelieveld and J. N. Crowley, NO_3 reactivity during a summer period in a temperate forest below and above the canopy, *Atmos. Chem. Phys.*, 2024, **24**, 8983–8997.
34 D. Mogensen, R. Gierens, J. N. Crowley, P. Keronen, S. Smolander, A. Sogachev, A. C. Nölscher, L. Zhou, M. Kulmala, M. J. Tang, J. Williams and M. Boy, Simulations of atmospheric OH, O_3 and NO_3 reactivities within and above the boreal forest, *Atmos. Chem. Phys.*, 2015, **15**, 3909–3932.
35 C. K. Thomas, A. Serafimovich, L. Siebicke, T. Gerken and T. Foken, in *Energy and Matter Fluxes of a Spruce Forest Ecosystem*, ed. T. Foken, Springer International Publishing, Cham, 2017, DOI: 10.1007/978-3-319-49389-3_6, pp. 113–135.

36 B. Schilperoort, M. Coenders-Gerrits, C. Jiménez Rodríguez, C. van der Tol, B. van de Wiel and H. Savenije, Decoupling of a Douglas fir canopy: a look into the subcanopy with continuous vertical temperature profiles, *Biogeosciences*, 2020, **17**, 6423–6439.

37 D. D. Baldocchi and T. P. Meyers, Turbulence structure in a deciduous forest, *Bound.-Layer Meteorol.*, 1988, **43**, 345–364.

38 M. Aubinet, C. Feigenwinter, B. Heinesch, Q. Laffineur, D. Papale, M. Reichstein, J. Rinne and E. Van Gorsel, in *Eddy Covariance: A Practical Guide to Measurement and Data Analysis*, ed M. Aubinet, T. Vesala and D. Papale, Springer Netherlands, Dordrecht, 2012, pp. 133–157, DOI: 10.1007/978-94-007-2351-1_5.

39 P. Dewald, C. M. Nussbaumer, J. Schuladen, A. Ringsdorf, A. Edtbauer, H. Fischer, J. Williams, J. Lelieveld and J. N. Crowley, Fate of the nitrate radical at the summit of a semi-rural mountain site in Germany assessed with direct reactivity measurements, *Atmos. Chem. Phys.*, 2022, **22**, 7051–7069.

40 H. Hellén, A. P. Praplan, T. Tykkä, I. Ylivinkka, V. Vakkari, J. Bäck, T. Petäjä, M. Kulmala and H. Hakola, Long-term measurements of volatile organic compounds highlight the importance of sesquiterpenes for the atmospheric chemistry of a boreal forest, *Atmos. Chem. Phys.*, 2018, **18**, 13839–13863.

41 S. T. Andersen, C. Nelson, L. Wüst, P. Dewald, G. N. T. E. Türk, J. Schuladen, H. Fischer, M. Ehn, I. Ylivinkka, L. R. Ahonen, T. Petäjä, Ü. Rannik, R. Rynek, H. Borsdorf, T. Mayer, J. Lelieveld and J. N. Crowley, Contribution of chemical reactions and deposition losses to the lifetimes and vertical gradients of O_3, *PAN and PAA in a Boreal Forest*, submitted, 2025.

42 P. Hari and M. Kulmala, Station for Measuring Ecosystem–Atmosphere Relations (SMEAR II), *Boreal Env. Res*, 2005, **10**, 315–322.

43 O. Peltola, T. Aslan, M. Aurela, A. Lohila, I. Mammarella, D. Papale, C. K. Thomas, T. Vesala and T. Laurila, Towards an enhanced metric for detecting vertical flow decoupling in eddy covariance flux observations, *Agric. For. Meteorol.*, 2025, **362**, 110326.

44 J. M. Liebmann, G. Schuster, J. B. Schuladen, N. Sobanski, J. Lelieveld and J. N. Crowley, Measurement of ambient NO_3 reactivity: Design, characterization and first deployment of a new instrument, *Atmos. Meas. Tech.*, 2017, **10**, 1241–1258.

45 IUPAC, *Task Group on Atmospheric Chemical Kinetic Data Evaluation*, ed. Ammann, M., Cox, R. A., Crowley, J. N., Herrmann, H., Jenkin, M. E., McNeill, V. F., Mellouki, A., Rossi, M. J., Troe, J. and Wallington, T. J., https://iupac.aeris-data.fr/en/home-english/, accessed 8 October 2025.

46 I. Tadic, J. N. Crowley, D. Dienhart, P. Eger, H. Harder, B. Hottmann, M. Martinez, U. Parchatka, J. D. Paris, A. Pozzer, R. Rohloff, J. Schuladen, J. Shenolikar, S. Tauer, J. Lelieveld and H. Fischer, Net ozone production and its relationship to nitrogen oxides and volatile organic compounds in the marine boundary layer around the Arabian Peninsula, *Atmos. Chem. Phys.*, 2020, **20**, 6769–6787.

47 C. M. Nussbaumer, U. Parchatka, I. Tadic, B. Bohn, D. Marno, M. Martinez, R. Rohloff, H. Harder, F. Kluge, K. Pfeilsticker, F. Obersteiner, M. Zoger, R. Doerich, J. N. Crowley, J. Lelieveld and H. Fischer, Modification of a conventional photolytic converter for improving aircraft measurements of NO_2 via chemiluminescence, *Atmos. Meas. Tech.*, 2021, **14**, 6759–6776.

48 J. Orphal, C. E. Fellows and P. M. Flaud, The visible absorption spectrum of NO_3 measured by high-resolution Fourier transform spectroscopy, *J. Geophys. Res. Atmos.*, 2003, 108.

49 S. T. Andersen, M. R. McGillen, C. Xue, T. Seubert, P. Dewald, G. N. T. E. Türk, J. Schuladen, C. Denjean, J. C. Etienne, O. Garrouste, M. Jamar, S. Harb, M. Cirtog, V. Michoud, M. Cazaunau, A. Bergé, C. Cantrell, S. Dusanter, B. Picquet-Varrault, A. Kukui, A. Mellouki, L. J. Carpenter, J. Lelieveld and J. N. Crowley, Measurement report: Sources, sinks, and lifetime of NO_x in a suburban temperate forest at night, *Atmos. Chem. Phys.*, 2024, **24**, 11603–11618.

50 H. T. Koponen, C. Escudé Duran, M. Maljanen, J. Hytönen and P. J. Martikainen, Temperature responses of NO and N2O emissions from boreal organic soil, *Soil Biol. Biochem.*, 2006, **38**, 1779–1787.

51 A. Bargsten, E. Falge, K. Pritsch, B. Huwe and F. X. Meixner, Laboratory measurements of nitric oxide release from forest soil with a thick organic layer under different understory types, *Biogeosciences*, 2010, **7**, 1425–1441.

52 M. A. Morris, D. Pagonis, D. A. Day, J. A. de Gouw, P. J. Ziemann and J. L. Jimenez, Absorption of volatile organic compounds (VOCs) by polymer tubing: implications for indoor air and use as a simple gas-phase volatility separation technique, *Atmos. Meas. Tech.*, 2024, **17**, 1545–1559.

53 P. Alekseychik, I. Mammarella, S. Launiainen, Ü. Rannik and T. Vesala, Evolution of the nocturnal decoupled layer in a pine forest canopy, *Agric. For. Meteorol.*, 2013, **174–175**, 15–27.

54 G. Jocher, J. Marshall, M. B. Nilsson, S. Linder, G. De Simon, T. Hörnlund, T. Lundmark, T. Näsholm, M. Ottosson Löfvenius, L. Tarvainen, G. Wallin and M. Peichl, Impact of Canopy Decoupling and Subcanopy Advection on the Annual Carbon Balance of a Boreal Scots Pine Forest as Derived From Eddy Covariance, *J. Geophys. Res.:Biogeosci.*, 2018, **123**, 303–325.

55 O. Peltola, K. Lapo and C. K. Thomas, A Physics-Based Universal Indicator for Vertical Decoupling and Mixing Across Canopies Architectures and Dynamic Stabilities, *Geophys. Res. Lett.*, 2021, **48**, e2020GL091615.

56 T. Vesala, T. Suni, Ü. Rannik, P. Keronen, T. Markkanen, S. Sevanto, T. Grönholm, S. Smolander, M. Kulmala, H. Ilvesniemi, R. Ojansuu, A. Uotila, J. Levula, A. Mäkelä, J. Pumpanen, P. Kolari, L. Kulmala, N. Altimir, F. Berninger, E. Nikinmaa and P. Hari, Effect of thinning

on surface fluxes in a boreal forest, *Global Biogeochem. Cycles*, 2005, **19**, GB2001.

57 I. Mammarella, P. Kolari, J. Rinne, P. Keronen, J. Pumpanen and T. Vesala, Determining the contribution of vertical advection to the net ecosystem exchange at Hyytiälä forest, Finland, *Tellus B*, 2007, **59**, 900–909.

58 M. L. Goulden, J. W. Munger, S.-M. Fan, B. C. Daube and S. C. Wofsy, Measurements of carbon sequestration by long-term eddy covariance: methods and a critical evaluation of accuracy, *Glob. Change Biol.*, 1996, **2**, 169–182.

59 A. G. Barr, A. D. Richardson, D. Y. Hollinger, D. Papale, M. A. Arain, T. A. Black, G. Bohrer, D. Dragoni, M. L. Fischer, L. Gu, B. E. Law, H. A. Margolis, J. H. McCaughey, J. W. Munger, W. Oechel and K. Schaeffer, Use of change-point detection for friction–velocity threshold evaluation in eddy-covariance studies, *Agric. For. Meteorol.*, 2013, **171–172**, 31–45.

60 G. Jocher, M. Fischer, L. Šigut, M. Pavelka, P. Sedlák and G. Katul, Assessing decoupling of above and below canopy air masses at a Norway spruce stand in complex terrain, *Agric. For. Meteorol.*, 2020, **294**, 108149.

61 A. Freundorfer, I. Rehberg, B. E. Law and C. Thomas, Forest wind regimes and their implications on cross-canopy coupling, *Agric. For. Meteorol.*, 2019, **279**, 107696.

62 H. Pleijel, G. Wallin, P. E. Karlsson and L. Skärby, Ozone gradients in a spruce forest stand in relation to wind speed and time of the day, *Atmos. Environ.*, 1996, **30**, 4077–4084.

63 P. E. Karlsson, M. Hansson, H. O. Höglund and H. Pleijel, Ozone concentration gradients and wind conditions in Norway spruce (Picea abies) forests in Sweden, *Atmos. Environ.*, 2006, **40**, 1610–1618.

64 J. Rinne, T. Markkanen, T. M. Ruuskanen, T. Petaja, P. Keronen, M. J. Tang, J. N. Crowley, U. Rannik and T. Vesala, Effect of chemical degradation on fluxes of reactive compounds –a study with a stochastic Lagrangian transport model, *Atmos. Chem. Phys.*, 2012, **12**, 4843–4854.

65 A. B. Guenther, P. R. Zimmerman, P. C. Harley, R. K. Monson and R. Fall, Isoprene and Monoterpene Emission Rate Variability - Model Evaluations and Sensitivity Analyses, *J. Geophys. Res. Atmos.*, 1993, **98**, 12609–12617.

66 F. Heintz, U. Platt, H. Flentje and R. Dubois, Long-term observation of nitrate radicals at the tor station, Kap Arkona (Rügen), *J. Geophys. Res. Atmos.*, 1996, **101**, 22891–22910.

67 S. S. Brown, H. Stark and A. R. Ravishankara, Applicability of the steady state approximation to the interpretation of atmospheric observations of NO_3 and N_2O_5, *J. Geophys. Res. Atmos.*, 2003, **108**, 4539.

68 H. Hu, H. Wang, K. Lu, J. Wang, Z. Zheng, X. Xu, T. Zhai, X. Chen, X. Lu, W. Fu, X. Li, L. Zeng, M. Hu, Y. Zhang and S. Fan, Variation and trend of nitrate radical reactivity towards volatile organic compounds in Beijing, China, *Atmos. Chem. Phys.*, 2023, **23**, 8211–8223.

69 J. N. Crowley, G. Schuster, N. Pouvesle, U. Parchatka, H. Fischer, B. Bonn, H. Bingemer and J. Lelieveld, Nocturnal nitrogen oxides at a rural mountain site in south-western Germany, *Atmos. Chem. Phys.*, 2010, **10**, 2795–2812.

70 K. Pilegaard, Processes regulating nitric oxide emissions from soils, *Philos. Trans. R. Soc. London, Ser. B*, 2013, **368**, 20130126.

71 E. R. Delaria, M. Vieira, J. Cremieux and R. C. Cohen, Measurements of NO and NO_2 exchange between the atmosphere and Quercus agrifolia, *Atmos. Chem. Phys.*, 2018, **18**, 14161–14173.

72 P. B. Shepson, J. W. Bottenheim, D. R. Hastie and A. Venkatram, Determination of the relative ozone and PAN deposition velocities at night, *Geophys. Res. Lett.*, 1992, **19**, 1121–1124.

73 H. Fischer, R. Axinte, H. Bozem, J. N. Crowley, C. Ernest, S. Gilge, S. Hafermann, H. Harder, K. Hens, R. H. H. Janssen, R. Konigstedt, D. Kubistin, C. Mallik, M. Martinez, A. Novelli, U. Parchatka, C. Plass-Dulmer, A. Pozzer, E. Regelin, A. Reiffs, T. Schmidt, J. Schuladen and J. Lelieveld, Diurnal variability, photochemical production and loss processes of hydrogen peroxide in the boundary layer over Europe, *Atmos. Chem. Phys.*, 2019, **19**, 11953–11968.

74 B. Bohn, Solar spectral actinic flux and photolysis frequency measurements in a deciduous forest, *J. Geophys. Res. Atmos.*, 2006, **111**, D15303.

75 J. Rinne, H. Hakola, T. Laurila and Ü. Rannik, Canopy scale monoterpene emissions of Pinus sylvestris dominated forests, *Atmos. Environ.*, 2000, **34**, 1099–1107.

76 J. Rinne, T. M. Ruuskanen, A. Reissell, R. Taipale, H. Hakola and M. Kulmala, On-line PTR-MS measurements of atmospheric concentrations of volatile organic compounds in a European boreal forest ecosystem, *Boreal Environ. Res.*, 2005, **10**, 425–436.

77 A. Ringsdorf, A. Edtbauer, J. Vilà-Guerau de Arellano, E. Y. Pfannerstill, S. Gromov, V. Kumar, A. Pozzer, S. Wolff, A. Tsokankunku, M. Soergel, M. O. Sá, A. Araújo, F. Ditas, C. Poehlker, J. Lelieveld and J. Williams, Inferring the diurnal variability of OH radical concentrations over the Amazon from BVOC measurements, *Sci. Rep.*, 2023, **13**, 14900.

78 E. R. Delaria, B. K. Place, A. X. Liu and R. C. Cohen, Laboratory measurements of stomatal NO_2 deposition to native California trees and the role of forests in the NO_x cycle, *Atmos. Chem. Phys.*, 2020, **20**, 14023–14041.

79 J. Aalto, P. Aalto, P. Keronen, P. Kolari, P. Rantala, R. Taipale, M. Kajos, J. Patokoski, J. Rinne, T. Ruuskanen, M. Leskinen, H. Laakso, J. Levula, T. Pohja, E. Siivola, M. Kulmala and I. Ylivinkka, *SMEAR II Hyytiälä forest meteorology, greenhouse gases, air quality and soil (Version 4)*, 2025, DOI: 10.23729/fd-933fd9fd-d31b-3e26-a01b-acef7901b843.

80 S. T. Andersen and P. Dewald, *BAIRN-VIP_2024_data*, Edmond, 2025, DOI: 10.17617/3.PBGFBI.

81 F. Crameri, *Scientific Colour Maps (8.0.1)*, Zenodo, 2023, DOI: 10.5281/zenodo.8409685.